IEEE Photonics Journal
An IEEE Photonics Society Publication

A Compact Two-Wavelength Time-Domain NIRS System Based on SiPM and Pulsed Diode Lasers

Volume 9, Number 1, February 2017

Mauro Buttafava, *Student Member, IEEE*
Edoardo Martinenghi, *Student Member, IEEE*
Davide Tamborini
Davide Contini
Alberto Dalla Mora
Marco Renna
Alessandro Torricelli
Antonio Pifferi
Franco Zappa, *Senior Member, IEEE*
Alberto Tosi, *Member, IEEE*

DOI: 10.1109/JPHOT.2016.2632061
1943-0655 © 2016 IEEE

A Compact Two-Wavelength Time-Domain NIRS System Based on SiPM and Pulsed Diode Lasers

Mauro Buttafava,[1] *Student Member, IEEE*, Edoardo Martinenghi,[2] *Student Member, IEEE*, Davide Tamborini,[1,3] Davide Contini,[2] Alberto Dalla Mora,[2] Marco Renna,[1] Alessandro Torricelli,[2,4] Antonio Pifferi,[2,4] Franco Zappa,[1] *Senior Member, IEEE*, and Alberto Tosi,[1] *Member, IEEE*

[1]Dipartimento di Elettronica, Informazione e Bioingegneria, Politecnico di Milano, Milan 20133, Italy
[2]Dipartimento di Fisica, Politecnico di Milano, Milan 20133, Italy
[3]Athinoula A. Martinos Center for Biomedical Imaging, MGH, Harvard Medical School, Charlestown, MA 02129 USA
[4]Istituto di Fotonica e Nanotecnologie, Consiglio Nazionale delle Ricerche, Milan 20133, Italy

DOI:10.1109/JPHOT.2016.2632061

Manuscript received November 12, 2016; accepted November 19, 2016. Date of current version December 22, 2016. This work was supported by the European Union's Horizon 2020 research and innovation programme under Grant 688303. This project is an initiative of the Photonics Public Private Partnership (www.photonics21.org). Corresponding author: M. Buttafava (e-mail: mauro.buttafava@polimi.it).

Abstract: This paper presents a complete, compact, and low power consumption instrument designed for time-domain near-infrared spectroscopy. It employs two custom-designed pulsed diode lasers (operating at 830 and 670 nm, with average optical power higher than 2 mW at 40 MHz repetition frequency), a single-photon detection module (based on a 1 mm^2 active area silicon photomultiplier), and a custom time-to-digital converter with 10 ps time resolution. The system experimental characterization shows an instrument response function narrower than 300 ps (full-width at half maximum), with measurement stability better than $\pm$1% over several hours of operation. The instrument, which is housed into a compact aluminum case (size 200 $\times$ 160 $\times$ 50 mm^3), is specifically tailored for portability and ease of operation, hence fostering the diffusion of time-domain diffuse optics techniques. Thanks to a total power consumption lower than 10 W, this system is suitable for battery operation, thus enabling on-field measurements.

Index Terms: Time-domain, diffuse optics, near-infrared spectroscopy, single-photon, silicon photomultiplier, pulsed diode laser, time-to-digital converter.

1. Introduction

Over the past few decades, the interest in non-invasive optical monitoring techniques is growing in several fields (e.g. biomedical, pharmaceutical, agricultural and chemical industry) as powerful tools for probing different properties of a medium [1]–[3]. Diffuse Optics (DO) investigates the photon propagation in highly scattering media, recovering information about their optical properties. Light

is typically injected into the sample through an optical fiber and the re-emitted signal is collected using another fiber, placed at a certain distance from the injection point.

The simplest implementation of DO instruments employs Continuous Wave (CW) illumination and detection [4], [5], having the advantage of low-complexity systems. However, in this approach a deep penetration of photons inside the sample can be obtained only by increasing the distance between light injection and collection points [6], at the expense of a reduced lateral resolution and a degradation of the Signal-to-Noise Ratio (SNR).

On the other hand, the Time Domain (TD) approach [7], [8] allows addition of a further dimension to the measurement, relying on the ability to acquire the photon Distribution of Times-of-Flight (DTOF) of a sample [9]. A TD scheme exploits the strong relationship between sample depth penetration and photon arrival times, which has the main advantage of a small dependence on injection and collection points separation [6], [10]. In fact, a reduction of this distance yields to an increased lateral resolution (which can reach its physical limit in case of null source-detector separation) [11]. Furthermore, by analyzing the recovered DTOF data, it is possible to distinguish between contributions coming from deeper structures of the sample and those related to more superficial ones [12]. The main drawback of TD diffuse optics is mainly due to the requirement of both sub-nanosecond pulsed light sources and time-resolved detection systems, which increase the system complexity [13].

Concerning the biomedical field, the demand for monitoring and imaging instrumentation based on DO techniques, in particular on Near-Infrared Spectroscopy (NIRS), is constantly increasing (e.g., in applications like functional brain imaging [14], muscle oximetry [15] and optical mammography [16]). Next generation NIRS instruments should offer top-class performance, ease of operation and reliability, in order to guarantee their wide diffusion in medical and diagnostic fields. Additionally, the design of compact and standalone systems can foresee the future development of wearable devices.

Up to now, instruments based on CW techniques are widespread, with clinically accepted applications and growing commercial interests, while new complex CW multichannel and wearable systems are under development [13]. Conversely, most of current TD NIRS instruments are custom-made prototypes [17], based on standalone commercial subsystems: pulsed laser modules, detection modules, Time-Correlated Single-Photon Counting (TCSPC) boards and custom optical components. Given this approach, they intrinsically exhibit scalability problems and high degree of complexity, thus strongly limiting their mass-diffusion, despites their better performance compared to CW systems. To the best of our knowledge, only few TD diffuse optics systems are commercially available. Among them, Hamamatsu Photonics K.K. developed the TRS-20 [18], [19], still based on bulky and fragile Photomultiplier Tubes (PMTs), and the most recent tNIRS-1 [20], which has been recently approved as a medical device in Japan. The latter is based on pulsed diode lasers operating at 9 MHz and Silicon Photomultipliers (SiPM) but exhibits a broad Instrument Response Function (IRF) of 1.5 ns Full-Width at Half Maximum (FWHM) and an acquisition time of 5 s.

This work aims at developing a new powerful TD NIRS instrument tailored for portability, reliability and ease of operation, with no compromise on performance. The system employs state-of-art light sources, detectors and timing electronics specifically designed for TD diffuse optics, representing the first step towards compact multichannel TD NIRS diagnostic instruments, for bed-side and wearable real-time monitoring applications.

2. Instrument Design

The presented system includes all the fundamental building blocks of a complete TD NIRS setup into a single instrument, with extremely compact dimensions ($200 \times 160 \times 50\,mm^3$) and weight (around 2 kg). Fig. 1 illustrates its block diagram, which includes i) two compact pulsed laser sources (at 830 nm and 670 nm wavelength) running alternately at 40 MHz repetition rate; ii) a single-photon detection module, based on a $1\,mm^2$ SiPM; iii) a control board, which also integrates the time-measurement electronics based on a Time-to-Digital Converter (TDC) ASIC (Application-Specific Integrated Circuit).

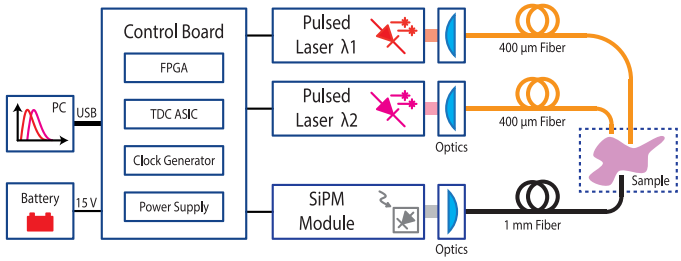

Fig. 1. Block diagram of the complete system. Light emitted from the two pulsed laser sources (at 670 nm and 830 nm) is injected into the sample with two 400 μm optical fibers. The optical response of the sample is collected via a single 1 mm fiber and focused on the 1 mm^2 active area of a SiPM-based single-photon detection module. A TDC-based TCSPC system is used to reconstruct the optical waveform with 10 ps resolution and send it in real-time to a portable computer for data analysis. The system consumes less than 10 W and can be battery-operated for on-field TD diffuse optics measurements.

Light is injected to and collected from the sample using three optical fibers, which are connected to SMA (Sub-Miniature A) ports. Custom optical systems launch the laser beams in two 400 μm multimode injection fibers and light re-emitted from the sample is collected using a 1 mm multimodal fiber and focused on the detector active area.

The instrument is able to directly acquire the DTOF of photons emitted from the tissue under test, which is reconstructed using the TCSPC technique (with 10 ps resolution). Each waveform histogram is transferred in real time to a remote Personal Computer (PC) via a Universal Serial Bus (USB) 2.0 link, for further data analysis. A custom control software is used to set all the measurement parameters and to monitor the system status. The entire instrument is powered from a single 15 V rail.

Following sections focus on the design of main building blocks of the system, namely, i) the two pulsed diode lasers, ii) the single-photon detection module and iii) the time-measurement and control systems. Each building block has been designed to push the instrument toward the limits of current technology but, at the same time, always paying attention to its size, reliability, robustness, and low power consumption as key parameters of a portable system.

2.1. Compact Pulsed Laser Sources

NIRS measurements require light sources with emission wavelengths in the 600–1000 nm spectral range, where absorption of tissue constituents is sufficiently low to allow for penetration of light through few centimeters from the surface [1]. At least two different wavelengths are needed, for example a first one between 670–690 nm and a second one between 810–830 nm for hemodynamics investigation [21]. FWHM of optical pulses must be lower than 250–300 ps, in order not to hamper the time resolution of the system, and the average optical power must be in the mW range, with repetition rates higher than 10–40 MHz, to shorten the overall measurement duration.

The targets of portability and reduced dimensions prevent the use of solid state and supercontinuum fiber-based laser sources, which are typically able to deliver average power of few Watts, with repetition rates up to 100 MHz and pulse durations below 10 ps FWHM, over a broad wavelength range [22], [23]. The most affordable light sources for portable TD diffuse optics instrumentation are pulsed diode lasers, which can provide average power in the order of few mW, with pulse width narrower than 500 ps and repetition rate up to 100 MHz [24], [25]. Lower output power and broader pulse width are greatly compensated by compactness, robustness, low power consumption, and good stability over time.

Commercial pulsed diode laser systems are available from different companies (e.g. PicoQuant GmbH, Becker&Hickl GmbH, A.L.S. GmbH, and others) and have already been successfully exploited in various TD NIRS systems [26], [27]. However, their dimensions would reduce the compact-

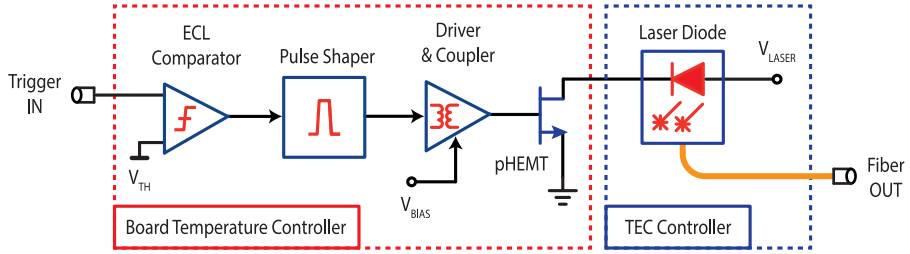

Fig. 2. Block diagram of the diode-based pulsed laser source. The trigger signal is fed to a low-jitter comparator and then to a pulse shaper. Voltage pulses between 500 ps and 5 ns arrive at the gate of a pHEMT transistor, via a pre-driving and coupling stage. The transistor is able to deliver current pulses up to 1 A to the laser diode at repetition rate up to 80 MHz. Each edge-emitting diode is enclosed in a 5.6 mm TO package mounted into an adjustable collimator, which is kept at a constant operating temperature (16–22 °C) through a TEC system. A heating system keeps the overall driving circuit at a constant temperature of about 45 °C to avoid any thermal drift and to speed-up the warm-up transient.

ness and portability of the instrument, in particular if multiple laser units (at multiple wavelengths) are needed.

For these reasons, the presented system exploits two custom-designed laser sources, based on laser diodes operated in gain-switching mode [28]. Fig. 2 shows a simplified schematic of these laser units: a trigger signal from the control board feeds a low-jitter Emitter-Coupled Logic (ECL) comparator, followed by a pulse shaper which shrinks the duration of each voltage pulse to 0.5–5 ns (adjustable, depending on the laser diode). A pre-driver combined with a radio-frequency coupler is used to switch ON and OFF a wide bandwidth pseudomorphic High Electron Mobility Transistor (pHEMT), delivering high-current pulses to the laser diode (up to 1 A peak current). A bias control voltage is used to set the proper sub-threshold current of the diode during the OFF state. The repetition frequency is adjustable in run-time from 100 kHz up to 80 MHz.

The main drawback of the gain switching operation is the strong relationship between light pulse shape and average optical power. Additionally, performance of these kind of pulsed laser sources is also strongly dependent on the employed diode. Test and selection of different devices have led to the choice of two medium-power 670 nm and 830 nm edge-emitting laser diodes. The 670 nm one can deliver light pulses of 240 ps FWHM with an average power of 2 mW, while the 830 nm one is able to provide 220 ps FWHM pulses with average power of 2.5 mW, when operated at 40 MHz (pulse widths are measured by directly coupling the collimated laser beam to the detector). The key advantage of the proposed driving circuit (compared to commercially available solutions) is the great flexibility, being able to accommodate any low to medium power laser diode, providing adjustable biasing and user-selectable repetition rate.

The employed laser diodes are housed in 5.6 mm TO packages, mounted into an adjustable optical collimator (Thorlabs Inc.). The free-space beams are then launched in two 400 μm multimode optical fibers, using two collimation packages on kinematic pitch/yaw mounts (Thorlabs Inc.). The obtained coupling efficiency is around 90%, from the laser package to the fiber output tip.

Another important requirement for a TD NIRS laser source is the stability over time and temperature. After a short warm-up time, any average power variation must remain lower than few percent (over the total measurement duration and environment temperature range) in order not to affect the measured data. Since laser diodes are extremely prone to temperature-related power fluctuations, a thermal control system has been implemented. It is divided in two different sections: i) a Thermoelectric Cooler (TEC) stabilizes the temperature of each laser diode with a set point between 16–22 °C and an error lower than 0.1 °C and ii) a linear heating circuit maintains the temperature of the driving electronics at ~45 °C, with an error lower than 0.5 °C. In this way, the laser operation is insensitive to ambient temperature variations (over a range from 15 °C to 35 °C) and the duration of warm-up transient is strongly reduced (requiring only 15 minutes). The overall laser diode driving

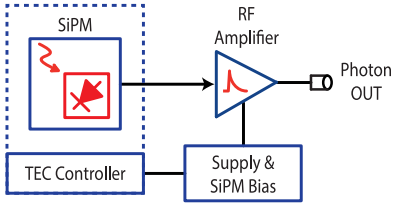

Fig. 3. Simplified block diagram of the detection module. The 1 mm^2 active area silicon photomultiplier is vacuum-sealed into a windowed TO-8 package, with a thermoelectric cooler that stabilizes its operating temperature at 10 °C. A microwave readout circuit amplifies the avalanche signal, achieving an overall single-shot precision better than 100 ps FWHM.

circuit is enclosed in a compact aluminum tube, with 25 mm diameter and 50 mm length, while the collimator and TEC assembly size is 20 $\times$ 15 $\times$ 20 mm^3.

2.2. SiPM-based Detection Module

Performance of the detection module is one of the key aspects in the design of TD NIRS instruments. Besides the fundamental request of single-photon sensitivity, a large active area (to maximize photon harvesting, by collecting most of the light from large optical fibers) and a good Photon Detection Efficiency (PDE) are also required: both parameters contribute to define the so-called "optical responsivity" of TD diffuse optics detectors [1]. The detector must also feature a good Single-Photon Timing Resolution (SPTR) in order to minimize the temporal jitter introduced in the reconstruction of DTOF curves. Finally, the detector has to be compact, low-cost and reliable, thus reducing both instrument complexity and cost. Therefore, vacuum-based photodetectors are not suitable for this instrument (due to their size and fragility), while solid-state detectors like Single-Photon Avalanche Diodes (SPADs) [29] are greatly advantaged in terms of detection efficiency, time resolution, power consumption and ease of operation. The main limitation of available SPADs is the small active area dimension, usually in the range of 20–200 μm of diameter [30]. However, it has been recently demonstrated [31] that a SiPM can effectively fit all the requirements of a TD NIRS detector. The state-of-art detection module exploited in the system, extensively described in [32], is based on a 1 mm^2 active area SiPM (commercially available from Excelitas Technologies) able to reach a PDE of 20% at 670 nm and 8% at 830 nm. Its simplified block diagram is shown in Fig. 3. SiPM is packaged with a TEC to maintain a stable working temperature of 10 °C, resulting in a Dark Counts Rate (DCR) of 90 kcps and a stability over time better than 1% on ambient temperature fluctuations. The readout circuit employs a Monolithic Microwave Integrated Circuits (MMIC) to amplify the avalanche signal with wide bandwidth (rise-time is about 1 ns) and negligible additional timing jitter. The output pulses amplitude is few hundreds of mV and their rising edges mark the arrival time of detected photons with an overall SPTR better than 100 ps FWHM.

2.3. Time-Measurement Electronics and Control Board

The optical response of a sample is obtained building the histogram of arrival times of each detected photon, with respect to the laser stimulus (thus reconstructing its DTOF waveform). The time elapsed between a laser pulse and the arrival of a single photon is recorded by the time-measurement electronics. Typical TCSPC time-interval meters usually provide few picoseconds resolution, with tens of nanoseconds measurement range [33], [34].

The instrument makes use of a state-of-art TDC ASIC (extensively described in [35]), fabricated in 0.35 μm CMOS (Complementary Metal-Oxide-Semiconductor) technology. This custom TDC, based on a single-stage Vernier delay loop interpolation, is able to measure time intervals with 10 ps resolution and 40 ps FWHM single-shot precision. The full-scale range is 160 ns and, with a conversion time of 150 ns, it can reach a conversion rate of 3 Mconv/s.

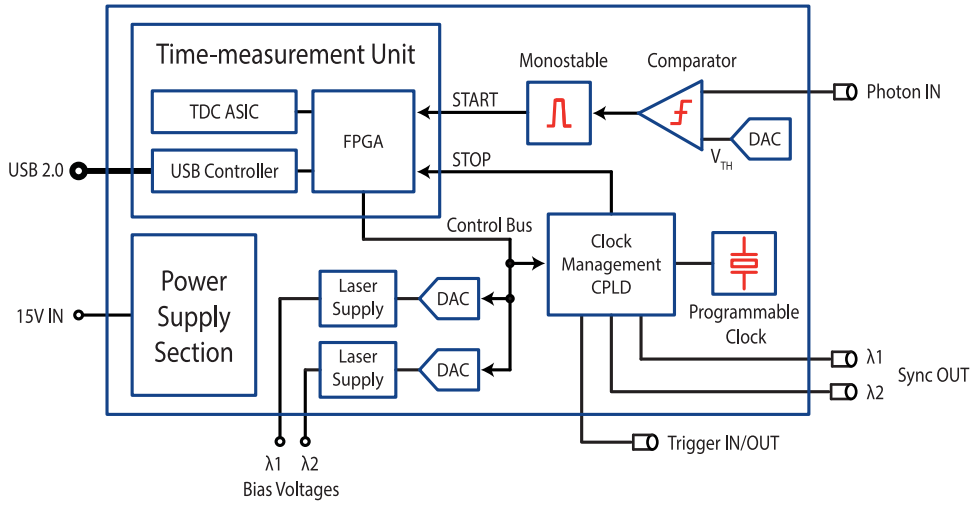

Fig. 4. Simplified block diagram of the instrument control board. Avalanche signals from the SiPM detection module are fed to a low jitter front-end circuit, composed by a wide-bandwidth comparator and a monostable circuit. The time-measurement unit, based on a 10 ps resolution custom TDC, measures the time interval elapsed between each detected photon and the corresponding excitation laser pulse. The embedded FPGA reconstructs the real-time optical waveform using the TCSPC technique and sends it to a remote PC, via USB 2.0 link. A CPLD-based clock management system alternatively activates the two laser sources, which are active one at a time. The repetition frequency is user-selectable between 100 kHz to 80 MHz and the integration time can be set from 0.5 s to 30 s for each measurement. The FPGA can also control the biasing of the two laser sources, enabling a fine adjustment of the light pulse shapes.

Fig. 4 shows the simplified block diagram of the instrument control board. The TDC chip is integrated in a standalone time-measurement unit, which also hosts a Spartan-6 (Xilinx Inc.) Field-Programmable Gate Array (FPGA) for data processing and system management, while a USB 2.0 controller is used for data communication with the remote PC. The time-measurement unit is an enhanced version of the system described in [36]. It receives the START of conversion pulse from the SiPM detection module (through a dedicated front-end circuit) and the STOP signal is a replica of the synchronization signal sent to the laser modules. The TDC measures the time elapsed between these two events and the FPGA builds a real-time histogram of the optical waveform in its internal memory. When a measurement is completed, the histogram is finally sent to the PC. To avoid dead times between consecutive measurements, the FPGA memory is segmented in two sectors: when the histogram is built in the first sector, a readout is performed on the second one and vice-versa. The integration time is user-selectable and can range between 0.5 s and 30 s.

The front-end circuit in Fig. 4 is designed to interface the SiPM detection module with the time-measurement unit. Rising edges of the amplified avalanche pulses are read using an ultra-low jitter ($<$10 ps RMS), high input bandwidth (8 GHz) comparator (Analog Devices Inc.) with adjustable threshold voltage, programmable using a 12-bit Digital-to-Analog Converter (DAC). The signal is then passed through a monostable circuit, which generates pulses of equal time duration and avoids retriggering of the time-measurement unit when a time conversion is running.

Synchronization signals for the laser sources and STOP signal for the TDC are generated from a clock-management circuit, based on a Complex Programmable Logic Device (CPLD) connected to a crystal-based programmable oscillator (Silicon Laboratories Inc.). The repetition frequency can be selected in a broad range, from 100 kHz to 80 MHz, with a typically used value of 40 MHz (for SiPM-based measurements). During an acquisition, the synchronization signal is alternately routed to the laser sources, which are active one at a time, while the corresponding histogram is built up. The synchronization signal can be also provided externally, using a dedicated trigger IN/OUT port (which acts as output terminal if the internal clock source is used).

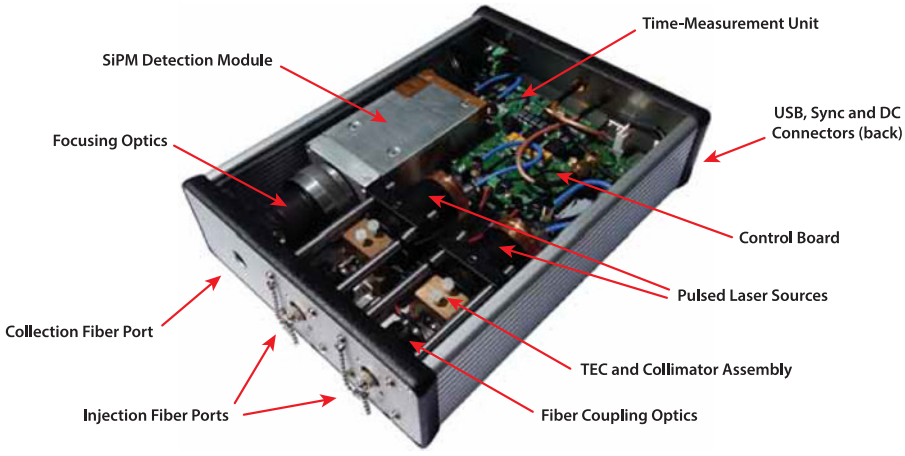

Fig. 5. Picture of the instrument. The front panel hosts the three fiber ports (one for collection and two for injection), while power supply, USB, and trigger IN/OUT connectors are on the rear panel. The instrument is enclosed in an aluminum box of size 200 $\times$ 160 $\times$ 50 mm^3.

Fig. 4 also shows the power supply stage of the laser sources: Two 12-bit DACs are used to control the bias point of each laser diode (with 10 mV resolution), in order to optimize their pulse shapes before each measurement.

The overall instrument is powered from a single 15 V rail and each operating voltage is derived from it, using high-efficiency DC/DC converters or linear regulators (when powering analog sections). The system can be directly operated using a 15 V lithium battery for on-field applications.

3. Experimental Characterization

The instrument prototype is shown in Fig. 5. Optical ports for injection and collection fibers are located on the front panel, while the rear panel hosts USB, power and trigger IN/OUT connectors. The system is housed in a robust aluminum box, with dimensions of 200 $\times$ 160 $\times$ 50 mm^3 and a total weight lower than 2 kg. Its power consumption is less than 10 W, giving the opportunity of battery operation, for on-field real-time measurements (as an example, using a 15 V–5 Ah Li-Ion battery, it is possible to acquire data for at least 7 hours). Following sections present the experimental characterization of the instrument and a TD NIRS measurement on solid phantoms for its validation.

3.1. Instrument Response Function

Typical instrument response functions of the system are shown in Fig. 6, for the 830 nm and 670 nm wavelengths. They are obtained by directly coupling collection and injection fibers, keeping the overall count rate of the detection module always below 2.5% of the lasers repetition rate (40 MHz), thus limiting the pile-up effect distortion well below 1% [37].

Each curve is obtained summing 30 measurements of 1 s duration (i.e. the equivalent integration time is 30 s) to increase the SNR and acquired data have been corrected for non-linearity of the time-measurement system (see Section 3.3). IRF widths are both below 300 ps FWHM, dominated by the widths of the two laser sources and the broadening of the light pulses, travelling through the 400 μm optical fibers. The contribution of SiPM module is about 100 ps FWHM [32], while the time-measurement electronics impacts for 40 ps FWHM [36]. The curve decay is slower at 830 nm, due to the longer diffusion tail of the SiPM at this wavelength [32].

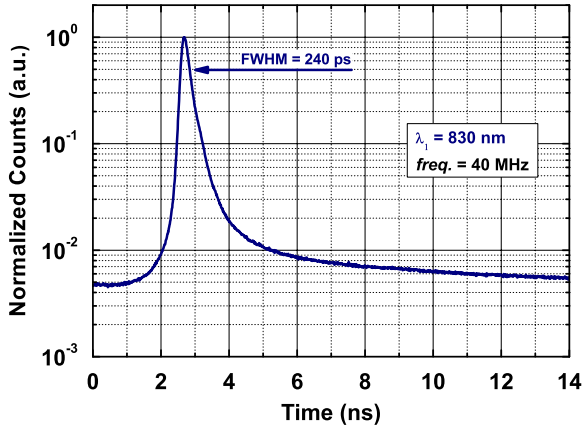

(a)

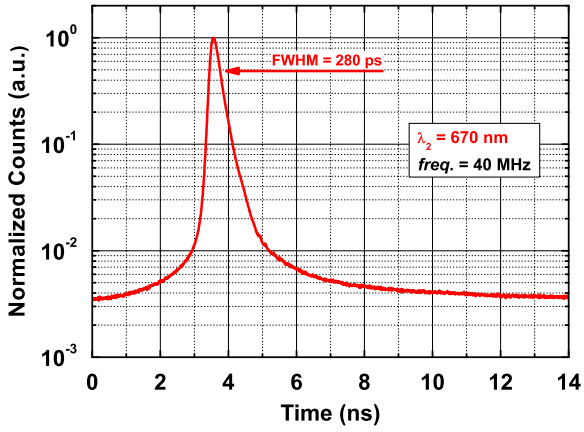

(b)

Fig. 6. Normalized instrument response function of the system for both 830 nm (a) and 670 nm (b) wavelengths. It is obtained by directly coupling collection and injection fibers, keeping the SiPM count rate lower than 2.5% of the 40 MHz laser repetition rate. FWHM is below 300 ps for both curves, mainly dominated by laser pulse widths and their broadening through injection fibers.

3.2. Stability

The stability of the instrument over time is a key aspect in long TD NIRS measurements. Any drift in terms of optical power of the laser sources, detection efficiency of the SiPM module or even time-measurement performance may affect the experimental results. This aspect is even more important if the target application of the NIRS system is related to continuous clinical monitoring. In addition, a reasonably short warm-up time of the instrument is desirable, in order to speed-up the measurement. The instrument has been tested for stability on a solid phantom (absorption of 0.1 cm^{-1} and reduced scattering of 10 cm^{-1}), recording the optical responses at the two wavelengths on a period of three hours, including the warm-up time. The distance between injection and collection fibers was 1.5 cm on the phantom surface and each DTOF curve was collected with an integration time of 1 s, interleaving the two laser sources. Variations of count rates over time account for potential drifts of either the laser sources or the detection module and remain below $\pm$1% for both the 830 nm and 670 nm lasers, after a warm-up time of 15 minutes, as shown in Fig. 7(a) and (d). The main contribution is due to the laser sources, since the detection module has shown variations lower than 1% in a broad range of temperatures [32]. Fig. 7(b), (e) show the shift of the centroid position of each curve: it is useful to evaluate potential drifts either in the laser driving circuits or in the time-measurement electronics. After the 15-minute warm-up time, performance is extremely

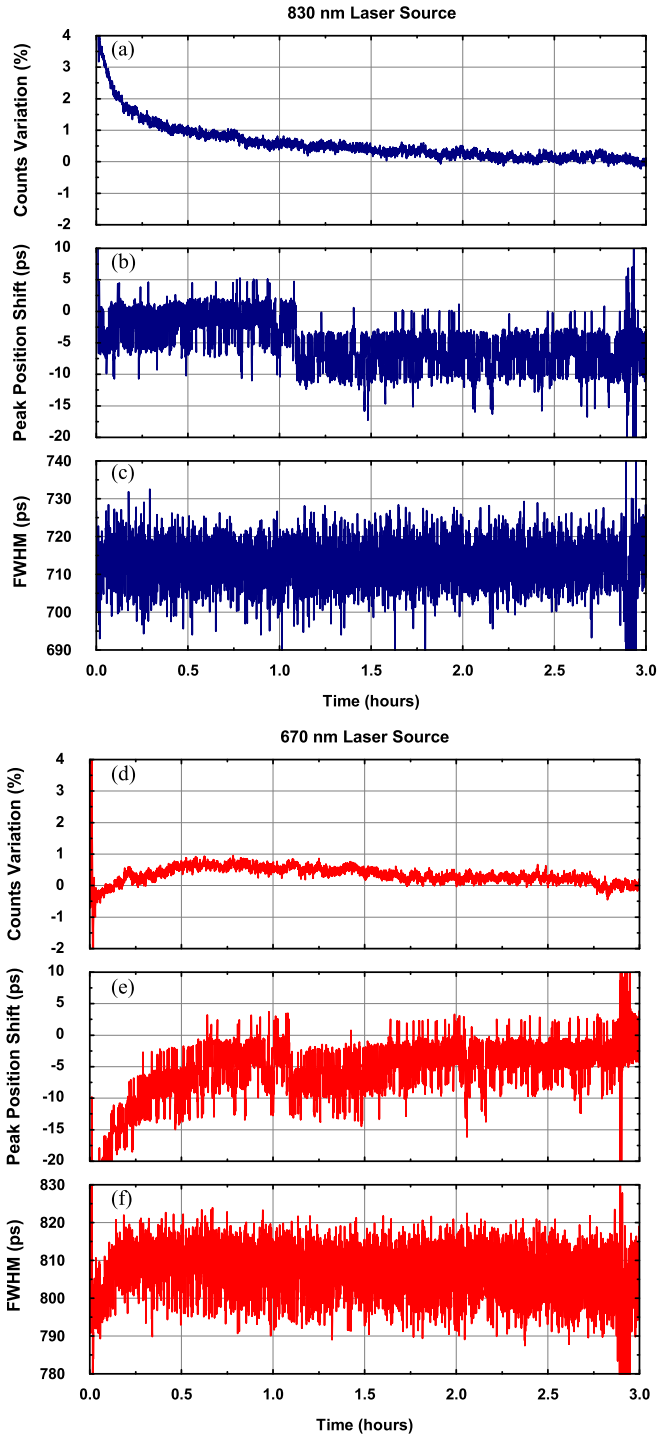

Fig. 7. Stability over time of the system. (a), (d) Count-rate variations for the 830 nm and 670 nm wavelengths, which reflect potential drifts of either the laser sources output power or the detection efficiency of the SiPM module. Variations remain below $\pm 1\%$ after a warm-up time of about 15 minutes. (b), (e) Centroid position of the recorded curves. (c), (f) Their temporal widths. These parameters account for drifts of both the laser driving circuits or the time-measurement system and exhibit very good performance.

good, with centroid variations of just few picoseconds (whose impact is an error of only few percent in the fitted absorption and reduced scattering coefficients). Finally, Fig. 7(c), (f) show the temporal widths of each recorded curve, which also present a very stable behavior (values in the order of 700–800 ps are due to optical parameters of the selected phantom).

3.3. Differential Non-Linearity Correction

A good linearity in the reconstruction of TCSPC waveforms is a mandatory requirement for TD diffuse optics instrumentation, especially for a precise estimation of the optical properties of the sample [1]. Non-linearity can usually arise from the time-measurement electronics, or can be induced by electromagnetic disturbances and crosstalk between various signals inside the system. The TDC ASIC exhibits extremely good performance, with an overall Differential Non-Linearity (DNL) lower than 1% (RMS) of the Least Significant Bit (LSB) [35]. Instead, the performance of the overall system can be estimated acquiring the count distribution over the measurement range, when injecting uncorrelated white light into the collection fiber. Ideally this distribution should remain perfectly flat, thanks to random arrival times of uncorrelated photons, and therefore any residual distortion is due to non-linearity. As shown in Fig. 8(a), the resulting measurement shows some oscillations in the counts distribution (with a time period around 1 ns), mainly due to signal crosstalk inside the FPGA, which translate into a total DNL of 3% (RMS).

To reduce this effect, it is possible to implement a form of DNL correction, by dividing the acquired TCSPC curves by a reference waveform (with mean value equal to one), which represents the shape of non-linearity over the measurement range. This reference waveform is created by integrating the count distribution, under uncorrelated illumination, for a long period (tens of minutes, in order to reduce the Poissonian noise), then normalizing it around its mean value. This technique can be effectively exploited thanks to the stability of the system, which allows to use the same reference waveform for long-term measurements without any degradation on the final results.

The effect of this correction on the same count distribution is visible in Fig. 8(b), where oscillations are mostly cancelled out, only remaining the residual white noise. Another way to look at the effect of the non-linearity correction is to compute the Fast Fourier Transform (FFT) of the two count distribution waveforms, as shown in Fig. 8(c). Uncorrected data clearly contain harmonics at frequencies below 3 GHz, which account for the mentioned crosstalk-based oscillations, while the spectrum of the corrected distribution is whited-out, with a slightly increased noise in the frequency range around 10 GHz due to the effect of numerical processing. Hence, applying (if needed) the correction algorithm to each acquired TCSPC curve before data processing (as done also for the IRFs of Fig. 6) allows to finally lower the equivalent DNL to about 1% (RMS).

3.4. Performance Assessment on Phantoms

To assess the system capability in retrieving the optical properties of homogeneous media, absorption and reduced scattering coefficients were measured on a series of solid phantoms [38]. They are made by a mixture of titanium dioxide particles (acting as scattering agent) and printer toner powder (acting as absorbing agent), embedded inside an epoxy resin matrix. A first series of four phantoms, labeled PA1, PA2, PA3, and PA4, presents an increasing nominal absorption coefficient, ranging from 0.07 to 0.28 cm^{-1} (in 0.07 cm^{-1} steps), and a constant reduced scattering coefficient of 10 cm^{-1}. Instead, a second series of three phantoms, labelled PS1, PS2 and PS3, has reduced scattering coefficients of 5, 10 and 15 cm^{-1} respectively, with a constant absorption coefficient of 0.07 cm^{-1}. Nominal values of the optical parameters were calculated on the basis of each phantom composition, knowing the calibration factors of the various compounds [38].

A reflectance configuration was employed, with injection and collection fibers placed on the phantom surface at a distance of 3 cm. Every measurement repetition was performed alternating the laser sources and had a duration of 1 s. The injected light power was properly attenuated to achieve no more than 10^6 counts per second (2.5% of the laser repetition frequency), therefore

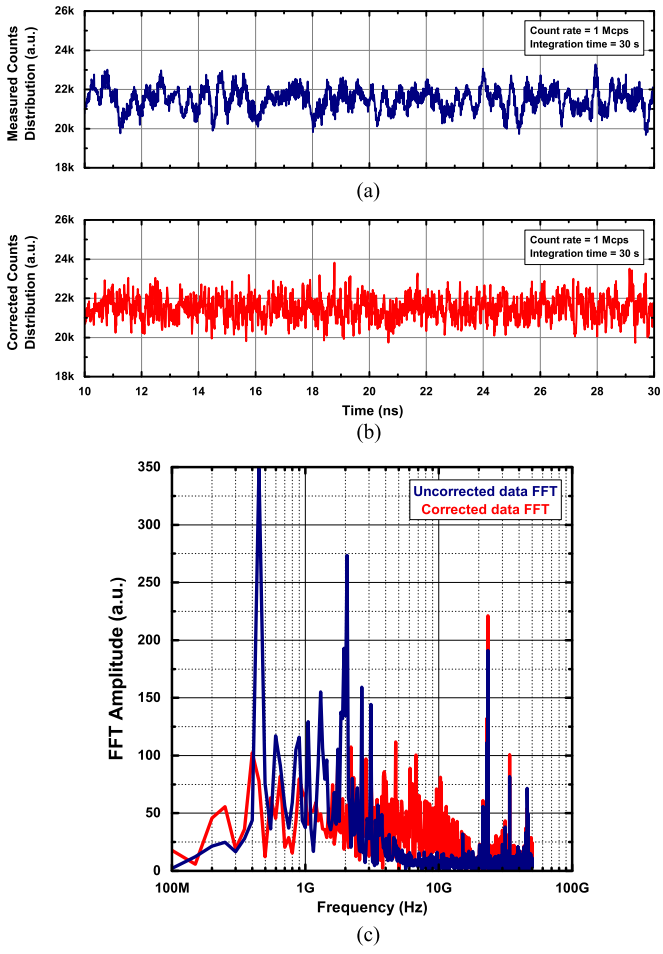

Fig. 8. Count distributions for uncorrelated illumination of the detector before (a) and after (b) the non-linearity correction. The intrinsic DNL of the TDC is lower than 1% of LSB (RMS). Due to signal crosstalk inside the FPGA, the overall DNL of the system increases to 3% of LSB (RMS) with the introduction of "low-frequency" oscillations (a). Thanks to their repeatability, it is, however, possible to implement a correction algorithm on the acquired curves, reducing the non-linearity due to these oscillations by at least a factor of 3 (b), as showed by the fast Fourier transform waveforms of (c), for the frequency range below 3 GHz.

avoiding any possible pile-up distortion [37]. Ten repetitions were performed for each phantom (and each wavelength), for averaging the calculated values.

Fig. 9(a) shows the normalized DTOF curves, obtained using the 670 nm laser source, for phantoms with varying absorption and constant reduced scattering. It is clearly visible how a higher absorption coefficient involves a steeper slope of the DTOF tail. Instead, Fig. 9(c) shows normalized DTOF curves at 670 nm for phantoms featuring an increasing scattering and constant absorption. It is worth noting how, in this case, a higher reduced scattering coefficient leads to a broadening of the DTOF, together with a delayed position of the peak.

Estimation of both absorption and reduced scattering coefficients is achieved by the best fitting of DTOF data, employing a standard model of diffusion theory [39]. The background noise is subtracted before the fitting procedure, evaluating its mean value preceding the beginning of each DTOF curve. Theoretical curves are convoluted with the IRF, for taking into account the non-idealities of the system. The fitting range is chosen between 90% of the DTOF peak value on the rising edge and 10% on the falling edge. The Levenberg-Marquardt algorithm is employed for error minimization by varying both absorption and reduced scattering coefficients.

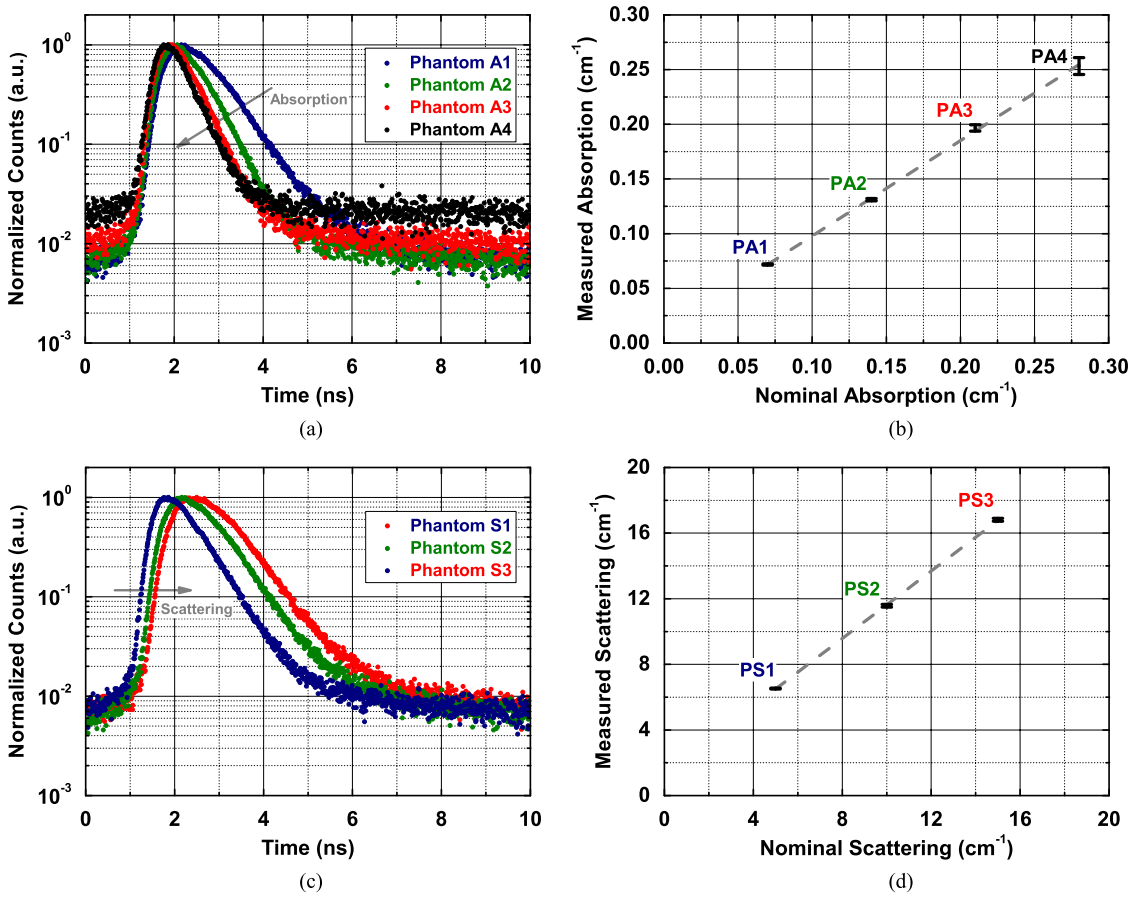

Fig. 9. Normalized DTOF curves for four different phantoms with increasing absorption (from 0.07 to 0.28 cm^{-1}) and constant reduced scattering (10 cm^{-1}) coefficients (a) and normalized DTOF curves for 3 different phantoms with increasing reduced scattering (from 5 to 15 cm^{-1}) and constant absorption (0.07 cm^{-1}) coefficients (c), acquired using the 670 nm laser source, with 1 s integration time, 10 repetitions, and a separation between injection and collection points of 3 cm. Average recovered absorption (b) and reduced scattering (d) coefficients are also plotted versus their nominal values. Error bars represent standard deviations calculated over the ten repetitions.

Results are shown in Fig. 9(b), (d), where the measured absorption and reduced scattering coefficients at 670 nm are plotted, highlighting the capability of the system to perfectly follow the linear trend of both parameters. Results are similar at the two wavelengths, so only data at 670 nm are reported.

4. Conclusions

We presented a compact time-domain near-infrared spectroscopy instrument, specifically designed for portability and ease of operation. The system is based on state-of-art components, including i) two pulsed diode lasers operating at 830 and 670 nm wavelengths, ii) a 1 mm^2 active area SiPM detection module, and iii) a time-measurement unit based on a 10 ps resolution TDC. The system characterization demonstrated an instrument response function of 240 ps and 280 ps for the 830 nm and 670 nm channels and an average light power of 2.5 mW and 2 mW respectively, when running at 40 MHz repetition rate. The FPGA-based architecture enables real-time acquisition and reconstruction of DTOF curves, which are downloaded to a remote PC for data processing. The system exhibits a measurement stability better than $\pm 1\%$ for operation times longer than several

hours and a non-linearity of the acquired waveforms lower than 1% of LSB (RMS). A performance assessment on phantoms was presented as experimental validation, showing the good linearity of the proposed system in recovering both absorption and reduced scattering parameters.

The instrument is ready for battery operation and, thanks to its compact size, flexibility, and customization possibilities, aims at becoming the first step towards portable multichannel and multi-wavelength TD NIRS diagnostic tools for bed-side and wearable applications.

References

[1] A. Pifferi, D. Contini, A. Dalla Mora, A. Farina, L. Spinelli, and A. Torricelli, "New frontiers in time-domain diffuse optics, a review," *J. Biomed. Opt.*, vol. 21, no. 9, pp. 091310-1–091310-17, 2016.

[2] T. Durduran, R. Choe, W. B. Baker, and A. G. Yodh, "Diffuse optics for tissue monitoring and tomography," *Rep. Progress Phys.*, vol. 73, no. 7, 2010, Art. no. 076701.

[3] A. P. Gibson and H. Dehghani, "Diffuse optical imaging," *Philos. Trans. A, Math. Phys. Eng. Sci.*, vol. 367, no. 1900, pp. 3055–3072, 2009.

[4] D. T. Delpy and M. Cope, "Quantification in tissue near-infrared spectroscopy," *Philos. Trans. R. Soc. London. Ser. B, Biol. Sci.*, vol. 352, no. 1354, pp. 649–659, 1997.

[5] H. Liu, D. A. Boas, Y. Zhang, A. G. Yodh, and B. Chance, "Determination of optical properties and blood oxygenation in tissue using continuous NIR light," *Phys. Med. Biol.*, vol. 40, no. 11, pp. 1983–1993, 1995.

[6] S. Del Bianco, F. Martelli, and G. Zaccanti, "Penetration depth of light re-emitted by a diffusive medium: Theoretical and experimental investigation," *Phys. Med. Biol.*, vol. 47, no. 23, pp. 4131–4144, 2002.

[7] P. Taroni, A. Pifferi, A. Torricelli, D. Comellia, and R. Cubeddu, "In vivo absorption and scattering spectroscopy of biological tissues," *Photochem. Photobiol. Sci.*, vol. 2, no. 2, pp. 124–129, 2003.

[8] A. Pifferi *et al.*, "Spectroscopic time-resolved diffuse reflectance and transmittance measurements of the female breast at different interfiber distances," *J. Biomed. Opt.*, vol. 9, no. 6, pp. 1143–1151, 2004.

[9] A. Liebert, H. Wabnitz, D. Grosenick, M. Möller, R. Macdonald, and H. Rinneberg, "Evaluation of optical properties of highly scattering media by moments of distributions of times of flight of photons," *Appl. Opt.*, vol. 42, no. 28, pp. 5785–5792, 2003.

[10] J. Steinbrink, H. Wabnitz, H. Obrig, A. Villringer, and H. Rinneberg, "Determining changes in NIR absorption using a layered model of the human head," *Phys. Med. Biol.*, vol. 46, no. 3, pp. 879–896, 2001.

[11] A. Pifferi *et al.*, "Time-resolved diffuse reflectance using small source-detector separation and fast single-photon gating," *Phys. Rev. Lett.*, vol. 100, no. 13, 2008, Art. no. 138101.

[12] L. Zucchelli, D. Contini, R. Re, A. Torricelli, and L. Spinelli, "Method for the discrimination of superficial and deep absorption variations by time domain fNIRS," *Biomed. Opt. Exp.*, vol. 4, no. 12, pp. 2893–2910, 2013.

[13] D. Contini *et al.*, "Review: Brain and muscle near infrared spectroscopy/imaging techniques," *J. Near Infrared Spectrosc.*, vol. 20, no. 1, pp. 15–27, 2012.

[14] A. Torricelli *et al.*, "Time domain functional NIRS imaging for human brain mapping," *Neuroimage*, vol. 85, pt 1, pp. 28–50, 2014.

[15] M. Wolf, M. Ferrari, and V. Quaresima, "Progress of near-infrared spectroscopy and topography for brain and muscle clinical applications," *J. Biomed. Opt.*, vol. 12, no. 6, 2007, Art. no. 062104.

[16] A. Pifferi, A. Farina, A. Torricelli, G. Quarto, R. Cubeddu, and P. Taroni, "Review: Time-domain broadband near infrared spectroscopy of the female breast: A focused review from basic principles to future perspectives," *J. Near Infrared Spectrosc.*, vol. 20, no. 1, pp. 223–235, 2012.

[17] A. Torricelli *et al.*, "Time domain functional NIRS imaging for human brain mapping," *Neuroimage*, vol. 85, no. 1, pp. 28–50, 2014.

[18] M. Oda *et al.*, "Near-infrared time-resolved spectroscopy system for tissue oxygenation monitor," *Proc. SPIE*, vol. 4160, pp. 204–210, 2000.

[19] K. Yoshitani *et al.*, "Clinical validity of cerebral oxygen saturation measured by time-resolved spectroscopy during carotid endarterectomy," *J. Neurosurg. Anesthesiol.*, vol. 25, no. 3, pp. 248–253, 2013.

[20] S. Fujisaka *et al.*, "A clinical tissue oximeter using NIR time-resolved spectroscopy," in *Proc. 43rd Annu. Meet. Int. Soc. Oxygen Transp. Tissue*, 2016, pp. 427–433.

[21] M. Ferrari, K. Norris, and M. Sowa, "Guest editorial: Medical near infrared spectroscopy 35 years after the discovery," *J. Near Infrared Spectrosc.*, vol. 20, pp. 7–9, 2012.

[22] A. Pifferi, A. Torricelli, P. Taroni, D. Comelli, A. Bassi, and R. Cubeddu, "Fully automated time domain spectrometer for the absorption and scattering characterization of diffusive media," *Rev. Sci. Instrum.*, vol. 78, no. 5, 2007, Art. no. 053103.

[23] NKT Photonics, "SuperK supercontinuum sources." [Online]. Available: http://www.nktphotonics.com/supercontinuum_sources. Accessed Jul. 15, 2016.

[24] PicoQuant GmbH, "LDH Series." [Online]. Available: http://www.picoquant.com/products/category/pulsed-lasers-and-leds. Accessed on: Jul. 15, 2016.

[25] Becker-Hickl GmbH, "BDS-MM Series." [Online]. Available: http://www.becker-hickl.de/bds-mm.htm. Accessed Jul.15, 2016.

[26] H. Wabnitz *et al.*, "A time-domain NIR brain imager applied in functional stimulation experiments," *Proc. SPIE*, vol. 58590, 2005, Art. no. 58590H.

[27] D. Contini *et al.*, "Multichannel time-resolved tissue oximeter for functional imaging of the brain," *IEEE Trans. Instrum. Meas.*, vol. 55, no. 1, pp. 85–90, Feb. 2006.

[28] P. Paulus, R. Langenhorst, and D. Jager, "Generation and optimum control of picosecond optical pulses from gain-switched semiconductor lasers," *IEEE J. Quantum Electron.*, vol. 24, no. 8, pp. 1519–1523, Aug. 1988.
[29] F. Zappa, S. Tisa, A. Tosi, and S. Cova, "Principles and features of single-photon avalanche diode arrays," *Sens. Actuators A, Phys.*, vol. 140, no. 1, pp. 103–112, 2007.
[30] F. Villa *et al.*, "CMOS SPADs with up to 500 μm diameter and 55% detection efficiency at 420 nm," *J. Mod. Opt.*, vol. 61, no. 2, pp. 102–115, 2014.
[31] A. Dalla Mora *et al.*, "Fast silicon photomultiplier improves signal harvesting and reduces complexity in time-domain diffuse optics," *Opt. Exp.*, vol. 23, pp. 13937–13946, 2015.
[32] E. Martinenghi, L. Di Sieno, D. Contini, M. Sanzaro, A. Pifferi, and A. Dalla Mora, "Time-resolved single-photon detection module based on silicon photomultiplier: A novel building block for time-correlated measurement systems," *Rev. Sci. Instrum.*, vol. 87, 2016, Art. no. 073101.
[33] Becker & Hickl GmbH, "SPC-130 Data-Sheet," Jul. 15, 2016. [Online]. Available: http://www.becker-hickl.de/spc130.htm
[34] PicoQuant GmbH, "PicoHarp300 Data-Sheet," Jul. 15, 2016. [Online]. Available: http://www.picoquant.com/products/category/tcspc-and-time-tagging-modules
[35] B. Markovic, S. Tisa, F. A. Villa, A. Tosi, and F. Zappa, "A high-linearity, 17 ps precision time-to-digital converter based on a single-stage Vernier delay loop fine interpolation," *IEEE Trans. Circuits Syst. I, Reg. Papers*, vol. 60, no. 3, pp. 557–569, Mar. 2013.
[36] D. Tamborini, M. Buttafava, A. Ruggeri, and F. Zappa, "Compact, low-power and fully reconfigurable 10 ps resolution, 160 μs range, time-resolved single-photon counting system," *IEEE Sensors J.*, vol. 16, no. 10, pp. 3827–3833, May 2016.
[37] W. Becker, *The Bh TCSPC Handbook*, 6th ed. Berlin, Germany: Becker & Hickl, 2014.
[38] A. Pifferi *et al.*, "Performance assessment of photon migration instruments: The MEDPHOT protocol," *Appl. Opt.*, vol. 44, no. 11, pp. 2104–2114, 2005.
[39] R. C. Haskell, L. O. Svaasand, T. T. Tsay, T. C. Feng, M. S. McAdams, and B. J. Tromberg, "Boundary conditions for the diffusion equation in radiative transfer," *J. Opt. Soc. Amer.*, vol. 11, pp. 2727–2741, 1994.